The Environment of Fe_4S_4 Clusters in Ferredoxins and High-Potential Iron Proteins. New Information from X-ray Crystallography and Resonance Raman Spectroscopy

Gabriele Backes,[1a] Yoshiki Mino,[1a,b] Thomas M. Loehr,[1a] Terrence E. Meyer,[1c] Michael A. Cusanovich,[1c] William V. Sweeney,[1d] Elinor T. Adman,[1e] and Joann Sanders-Loehr*,[1a]

Contribution from the Department of Chemical and Biological Sciences, Oregon Graduate Institute of Science and Technology, Beaverton, Oregon 97006-1999, Department of Biochemistry, University of Arizona, Tucson, Arizona 85721, Department of Chemistry, City University of New York, Hunter College, New York, New York 10021, and Department of Biological Structure, University of Washington, Seattle, Washington 98195.
Received May 7, 1990

Abstract: A comparison of ferredoxin (Fd) crystal structures from *Peptococcus aerogenes*, *Bacillus thermoproteolyticus*, and *Azotobacter vinelandii* shows that the polypeptide chain folding in the vicinity of each of the $[Fe_4S_4(Cys)_4]^{2-}$ clusters is highly conserved with regard to the location of the four cysteine ligands, the cysteine dihedral angles, and the eight amide NH groups that hydrogen bond to sulfur atoms of the cluster. Resonance Raman spectra of Fds from *Clostridium pasteurianum* and *Clostridium acidi-urici* exhibit a set of seven peaks assignable to Fe–S(bridging) vibrations and three peaks assignable to Fe–S(Cys) vibrations, as expected from the D_{2d} distortion of the clusters observed in the X-ray structures. Hydrogen bonding of the bridging and terminal sulfur ligands has been verified by shifts in Fe–S vibrational frequencies in D_2O. The solvent accessibility of the Fe_4S_4 clusters due to protein breathing motion is evident from the similarity of the isotope shifts between native Fd and protein equilibrated with deuterium prior to cluster reconstitution. Since the cluster geometry and hydrogen bonds are highly conserved in ferredoxins, their ~400-mV range in redox potentials must be due to different amino acid side chains in the vicinity of the clusters and to varying degrees of exposure to solvent. The crystal structure of the high-potential iron protein (HiPIP) from *Chromatium vinosum* reveals that, despite the presence of an $[Fe_4S_4(Cys)_4]^{2-}$ cluster, there is no evolutionary relationship to the Fds in amino acid sequence, polypeptide chain folding, location of cysteine ligands, cysteine dihedral angles, or the five hydrogen bonds from amide NH groups. Resonance Raman spectra of reduced HiPIPs from *Chromatium*, *Rhodocyclus*, *Rhodopila*, and *Ectothiorhodospira* show a set of six Fe–S^b (bridging) vibrations that are remarkably similar to those of the ferredoxins. These results lend strong support to X-ray crystallographic findings of similar D_{2d}-distorted iron–sulfur clusters in Fds and HiPIPs and argue against the suggestion (Czernuszewicz, R. S.; Macor, K. A.; Johnson, M. K.; Gewirth, A.; Spiro, T. G. *J. Am. Chem. Soc.* **1987**, *109*, 7178) that HiPIPs have a more symmetric cluster geometry than Fds. The increased number and vibrational frequency of Fe–S(Cys) modes in HiPIPs is ascribed to coupling of Fe–S(Cys) stretching modes with S–C–C deformations, which is facilitated by the presence of an ~180° Fe–S_γ–C_β–C_α dihedral angle in HiPIP. Deuterium exchange in *C. vinosum* HiPIP results in frequency shifts in the Fe–S(Cys) modes similar to those seen for Fds, consistent with the X-ray finding of four H bonds to cysteine sulfurs. However, in contrast to Fd, exchange of these hydrogen-bonded amide NH groups requires partial unfolding of the protein, confirming that the cluster in native HiPIP is inaccessible to water. The preference for the $[Fe_4S_4(Cys)_4]^{1-}$ oxidation level (i.e., lower net charge on the cluster) in HiPIPs is ascribed primarily to the hydrophobic environment of the cluster and the smaller number of hydrogen bonds relative to ferredoxins.

Introduction

Iron–sulfur proteins of the $Fe_4S_4(Cys)_4$ variety are among the most widely distributed metalloprotein electron carriers in nature.[2] They are involved in a number of biologically important redox processes including photosynthesis, nitrogen fixation, and respiration.[3] Ferredoxins (Fds) cycle between the $[Fe_4S_4(Cys)_4]^{2-/3-}$ states at negative potentials that range from −250 to −650 mV.[4] In contrast, the high-potential iron proteins (HiPIPs) function at positive potentials of +50 to +450 mV for their $[Fe_4S_4(Cys)_4]^{1-/2-}$ oxidation levels.[5] The redox potential for the reduction of HiPIPs to the 3− state is considerably lower than −600 mV, and this form cannot be achieved under normal physiological conditions.[6] Likewise, the ferredoxins cannot be oxidized to the 1− state without destruction of the iron–sulfur cluster.

The enormous diversity in the potentials of the accessible oxidation states in these two classes of $Fe_4S_4(Cys)_4$ proteins has sparked interest in the discovery of possible differences in the iron–sulfur sites. X-ray crystal structures have been determined for oxidized and reduced HiPIPs from *Chromatium vinosum*[7] and for oxidized ferredoxins from *Peptococcus aerogenes*,[8] *Azotobacter vinelandii*,[9,10] and *Bacillus thermoproteolyticus*.[11] In each case, the iron and sulfido groups are arranged in a slightly distorted cube with each iron additionally connected to a cysteinyl sulfur of the polypeptide chain. The $[Fe_4S_4(Cys)_4]^{2-}$ centers in the reduced HiPIP and the three oxidized Fds exhibit similar Fe–S bond distances and bond angles for the bridging and terminal sulfur atoms. Most of the above $[Fe_4S_4(Cys)_4]^{2-}$ clusters show

(1) (a) Oregon Graduate Institute of Science and Technology. (b) Present address: Osaka University of Pharmaceutical Sciences, Matsubara, Osaka 580, Japan. (c) University of Arizona. (d) City University of New York. (e) University of Washington.

(2) Thompson, A. J. In *Metalloproteins*; Harrison, P., Ed.; Verlag Chemie: Weinheim, FRG, 1985; Part 1, pp 79–120.

(3) Thauer, R. K.; Schoenheit, P. In *Iron–Sulfur Proteins*; Spiro, T. G., Ed.; Wiley Interscience: New York, 1982; pp 329–342.

(4) (a) Yoch, D. C.; Carithers, R. P. *Microbiol. Rev.* **1979**, *43*, 384–421. (b) Armstrong, F. A.; George, S. J.; Thomson, A. J.; Yates, M. G. *FEBS Lett.* **1988**, *234*, 107–110.

(5) Meyer, T. E.; Przysiecki, C. T.; Watkins, J. A.; Bhattacharyya, A.; Simondsen, R. P.; Cusanovich, M. A.; Tollin, G. *Proc. Natl. Acad. Sci. U.S.A.* **1983**, *80*, 6740–6744.

(6) Cammack, R. *Biochem. Biophys. Res. Commun.* **1973**, *54*, 548–554.

(7) (a) Carter, C. W., Jr.; Kraut, J.; Freer, S. T.; Alden, R. A. *J. Biol. Chem.* **1974**, *249*, 6339–6346. (b) Carter, C. W., Jr. In *Iron–Sulfur Proteins*; Lovenberg, W., Ed.; Academic Press: New York, 1977; pp 157–204.

(8) (a) Adman, E. T.; Sieker, L. C.; Jensen, L. H. *J. Biol. Chem.* **1973**, *248*, 3987–3996. (b) Adman, E. T.; Sieker, L. C.; Jensen, L. H. *J. Biol. Chem.* **1976**, *251*, 3801–3806.

(9) Stout, G. H.; Turley, S.; Sieker, L. C.; Jensen, L. H. *Proc. Natl. Acad. Sci. U.S.A.* **1988**, *85*, 1020–1022.

(10) Stout, C. D. *J. Mol. Biol.* **1989**, *205*, 545–555.

(11) (a) Fukuyama, K.; Nagahara, Y.; Tsukihara, T.; Katsube, Y. *J. Mol. Biol.* **1988**, *199*, 183–193. (b) Fukuyama, K.; Matsubara, H.; Tsukihara, T.; Katsube, Y. *J. Mol. Biol.* **1989**, *210*, 383–398.

0002-7863/91/1513-2055$02.50/0

a tetragonal compression along an S_4-rotation axis, as do $[Fe_4S_4(SR)_4]^{2-}$ models,[12] resulting in a cluster symmetry of D_{2d} or lower instead of pure tetrahedral T_d. A resonance Raman (RR) spectroscopic analysis has confirmed the D_{2d} distortion in both $Fe_4S_4(Cys)_4$ clusters of *Clostridium pasteurianum* Fd, but has questioned the degree of distortion in *C. vinosum* HiPIP.[13] In this work, we present the RR spectra of HiPIPs from three other organisms and conclude that the D_{2d} distortion is a common feature of all protein $Fe_4S_4(Cys)_4$ cores.

Because the structures of the iron–sulfur clusters in ferredoxins and HiPIPs appear to be so nearly identical, attention has turned to the likelihood that it is the *cluster environment* that influences the redox potential. The crystallographic data indicate that the Fe_4S_4 clusters are considerably closer to the protein surface in the Fds than they are in the HiPIPs. The more buried nature of the HiPIP cluster has been corroborated by electron spin echo studies, which indicate that hydrogens in the vicinity of the Fd clusters exchange with deuterium in the solvent, whereas hydrogens in the vicinity of the HiPIP cluster do not.[14] This implies that protein breathing makes the Fe_4S_4 clusters in Fd accessible to aqueous solvent and potential hydrogen-bonding interactions, whereas the Fe_4S_4 cluster in HiPIP is more rigidly positioned inside the protein. Unfolding of HiPIP in 80% DMSO–20% H_2O increases the water exposure of the cluster and shifts the redox potentials into the Fd range.[6] It is likely that the more buried environment of the cluster in native HiPIP favors a lower net charge and, thus, is a major factor in promoting the 1– oxidation state of HiPIP.

Aside from cluster interactions with aqueous solvent, the redox potential of $Fe_4S_4(Cys)_4$ proteins may also be influenced by hydrogen bonds to the sulfur ligands from the polypeptide chain. Hydrogen bonding of internal polar groups is a general phenomenon in protein structures.[15] It has been noted that the Fe_4S_4 clusters in *P. aerogenes* Fd are involved in more hydrogen bonds than the cluster in *C. vinosum* HiPIP and that the larger number of hydrogen bonds in Fd could stabilize the more negatively charged $[Fe_4S_4(Cys)_4]^{3-}$ reduced state.[16,17] However, the relative importance of hydrogen bonding has been questioned on the basis of the absence of a deuterium effect on the redox potential of ferredoxin[18a] and a poor correlation of redox potential with NMR-detectable hydrogen bonds in HiPIPs.[18b]

The original hypothesis regarding the differential number of hydrogen bonds was based on the X-ray structures of one ferredoxin and one HiPIP.[16] We have now reevaluated the refinement of the original *P. aerogenes* Fd model and compared our results to the recently determined *A. vinelandii* and *B. thermoproteolyticus* Fd structures. We find that the large number of hydrogen bonds in ferredoxins is a highly conserved feature. We have also utilized the occurrence of deuterium isotope shifts in the resonance Raman spectrum[19] to estimate the relative hydrogen bond strengths. We conclude that the 3-fold larger number of NH···S bonds to bridging sulfides in Fd is likely to play a role in stabilizing the lower oxidation state of Fd relative to HiPIP. In contrast, the apparent constancy of cluster hydrogen bonds in ferredoxins indicates that the ~400-mV variability in Fd redox potentials must be ascribed to other factors such as cluster environment.

Experimental Procedures

Ferredoxins. The preparation of crystals of *Peptococcus aerogenes* (*Pa*) Fd has been described previously.[8a] *Clostridium pasteurianum* (*Cp*) and *Clostridium acidi-urici* (*Ca*) were grown and Fds isolated according to the procedure of Rabinowitz.[20] For deuterium isotope exchange, *Cp* and *Ca* Fds were first converted to the apo form according to the procedure of Hong and Rabinowitz,[21] using 10% (w/v) trichloroacetic acid. The lyophilized proteins were dissolved in unbuffered solutions of H_2O or D_2O, incubated at 4 °C for ~24 h, and then lyophilized again. Samples were reconstituted in H_2O or D_2O according to the procedure of Hong and Rabinowitz.[21] For reconstitution from D_2O, deuterated urea was used. Samples were concentrated to ~2 mM by ultrafiltration. Native *Cp* and *Ca* ferredoxins were also exposed directly to D_2O buffer by several cycles of dilution and ultrafiltration (Centricon PM-10), followed by an 18-h incubation at 4 °C.

High-Potential Iron Proteins. Proteins were obtained from *Chromatium vinosum* (*Cv*), *Rhodopila globiformis* (*Rg*), *Rhodocyclus tenuis* (*Rt*) strain 2761, and *Ectothiorhodospira halophila* (*Eh*), isozyme 1, as described previously.[22] Owing to a recent change in nomenclature,[23] *Rg* and *Rt* correspond to organisms previously referred to as *Rhodopseudomonas globiformis* and *Rhodospirillum tenue*, respectively.

To allow complete exchange of hydrogens located near the active site, *Cv* HiPIP was exposed to partly denaturing conditions.[14] A concentrated protein solution was diluted 10-fold in 0.05 M potassium phosphate buffer in H_2O or D_2O (pH reading 7.5) and reconcentrated by centrifugation in a Centricon 10 (Amicon). This process was repeated twice to give ~2 mM protein. Under strictly anaerobic conditions, a freshly distilled dry DMSO solution was slowly added to the protein to yield a final concentration of 80% DMSO. The protein was incubated for 20–120 min for complete exchange. Refolding was achieved by diluting the DMSO concentration to 40% by the slow addition of buffer. The DMSO was then removed by anaerobic dialysis at 4 °C against phosphate buffer. The protein was exposed to air and concentrated again in a Centricon 10 unit. On the basis of the absorption spectrum, the recovery of *Cv* $HiPIP_{red}$ was close to 100% with the same A_{388}/A_{282} as the starting material. Oxidation was accomplished by treatment with 2 mM $K_3Fe(CN)_6$.

Resonance Raman Spectroscopy. Raman spectra were collected on a computer-interfaced Jarrell-Ash spectrophotometer equipped with Spectra-Physics 164-05 (Ar) and 2025-11 (Kr) lasers, a Coherent Innova 90-6 Ar ion laser, an RCA C31034 photomultiplier tube, an Ortec Model 9302 amplifier/discriminator, and a recently upgraded computer (Intel 310). Spectra were obtained by ~150° backscattering from samples at 15 K frozen onto a gold-plated sample holder of a closed-cycle helium Displex (Air Products) or at 90 K in capillaries inserted into the copper cold-finger of a liquid N_2 filled Dewar. Deuterium isotope shifts were determined on spectra collected under identical conditions. Peak positions were obtained by either abscissa expansion or curve fitting. The reported isotope shifts ($\Delta\nu$) are reproducible to within ± 0.7 cm^{-1}.

X-ray Crystallographic Refinement. The same data set collected for the earlier refinement of *P. aerogenes* ferredoxin at 2.0 Å[8b] was used. The programs of Hendrickson and Konnert[24] were applied, starting with the earlier refined model and adding new solvent molecules at appropriate sites. While the previous agreement between observed and calculated structure factors reached 0.188, quite satisfactory for the time, it presently stands at 0.137, with only 86 solvent positions instead of 146. Full details of the refinement will be published elsewhere.

Results and Discussion

Core Structures from X-ray Crystallography and Raman Spectroscopy. High-resolution X-ray structures are available for a number of synthetic analogues of the $[Fe_4S_4(Cys)_4]^{2-}$ core.[12] In most cases, there is a tetragonal compression of the Fe_4S_4 cube resulting in four short and eight long Fe–S^b (bridging sulfide) bonds and a cluster geometry that is closer to D_{2d} than T_d. The X-ray structures of oxidized ferredoxin from *P. aerogenes* and reduced HiPIP from *C. vinosum* have been interpreted as showing

(12) Berg, J. M.; Holm, R. H. In *Iron-Sulfur Proteins*; Spiro, T. G., Ed.; Wiley: New York, 1982; pp 1–66.
(13) Czernuszewicz, R. S.; Macor, K. A.; Johnson, M. K.; Gewirth, A.; Spiro, T. G. *J. Am. Chem. Soc.* **1987**, *109*, 7178–7187.
(14) Orme-Johnson, N. R.; Mims, W. B.; Orme-Johnson, W. H.; Bartsch, R. G.; Cusanovich, M. A.; Peisach, J. *Biochim. Biophys. Acta* **1983**, *748*, 68–72.
(15) Baker, E. N.; Hubbard, R. E. *Prog. Biophys. Mol. Biol.* **1984**, *44*, 97–179.
(16) Adman, E. T.; Watenpaugh, K. D.; Jensen, L. H. *Proc. Natl. Acad. Sci. U.S.A.* **1975**, *72*, 4854–4858.
(17) Sheridan, R. P.; Allen, L. C.; Carter, C. W., Jr. *J. Biol. Chem.* **1981**, *256*, 5052–5057.
(18) (a) Sweeney, W. V.; Magliozzo, R. S. *Biopolymers* **1980**, *19*, 2133–2141. (b) Krishnamoorthi, R.; Markley, J. L.; Cusanovich, M. A.; Przysiecki, C. T.; Meyer, T. E. *Biochemistry* **1986**, *25*, 60–67.
(19) Mino, Y.; Loehr, T. M.; Wada, K.; Matsubara, H.; Sanders-Loehr, J. *Biochemistry* **1987**, *26*, 8059–8065.
(20) Rabinowitz, J. C. *Methods Enzymol.* **1972**, *24*, 431–446.
(21) Hong, J.-S.; Rabinowitz, J. C. *Biochem. Biophys. Res. Commun.* **1967**, *29*, 246–252.
(22) (a) Bartsch, R. G. *Methods Enzymol.* **1978**, *53*, 329–340. (b) Meyer, T. E. *Biochim. Biophys. Acta* **1985**, *806*, 175–183. (c) Tedro, S.; Meyer, T. E.; Kamen, M. S. *J. Biol. Chem.* **1976**, *251*, 129–136.
(23) Imhoff, J. F.; Trüper, H. G.; Pfennig, N. *Int. J. Syst. Bacteriol.* **1984**, *34*, 340–343.
(24) Hendrickson, W. A.; Konnert, J. H. In *Computing in Crystallography*; Diamond, R., Ramaseshan, S., Venkatesan, K., Eds.; Indian Academy of Sciences: Bangalore, India, 1980; pp 13.01–13.23.

Table I. Resonance Raman Frequencies for Ferredoxins and HiPIPs[a]

D_{2d} assgnmnt[b]	Fd_{ox}		$HiPIP_{red}$				$HiPIP_{ox}$			
	Cp	*Ca*	*Rg*	*Cv*	*Rt*	*Eh*	*Rg*	*Cv*	*Rt*	*Eh*
B_2 (Br)	250	255	250	250	250	250	250	251	251	250
A_2 (Br)	267	266	264	262		266	267	273	269	
E (Br)	276	278	275	275	276	270	277		280	
B_1 (Br)	283	285	286	292						
A_1 (Br)	298	300	297	299	295	297	297	300	299	296
A_1 (Br)	338	339	338	339	340	336	341	344	343	341
B_2 (T)	352	350	361	358	364	360	373	376	373	371
E (T)	364	366	369	362	370		382	390	389	
B_2 (Br)	379	379								
(T)			386	391	384	384	397	403	400	393
A_1 (T)	395[c]	397	395	396	399	393		410	413	410
(T)							417	425	421	

[a] Frequencies in reciprocal centimeters. [b] Assignments for *Cp* Fd from ref 13. (Br), bridging Fe–S^b mode; (T), terminal Fe–S^t(Cys) mode. Analogous assignments for $HiPIP_{ox}$ and $HiPIP_{red}$ based on present results and ref 29. Larger number of Fe–S^t modes in HiPIPs due to coupling with δ(Cys). [c] Mode in *Cp* Fd has a substantial amount of bridging character based on frequency shifts with bridging ^{34}S and Se (ref 26).

similar tetragonal compressions of the Fe_4S_4 clusters.[25] In the present refinement of the *Pa* Fd structure, the four short Fe–S bonds in cluster I average 2.27 Å relative to average distances of 2.29 and 2.30 Å in the other two dimensions; the respective values for cluster II are 2.26, 2.26, and 2.32 Å. The root-mean-squared bond distances for the 24 Fe–S^b bonds and the eight Fe–S^t (terminal sulfide) bonds are 2.28 ± 0.05 and 2.26 ± 0.06 Å, respectively, so that the extent of deformation is really quite small.

(a) Ferredoxins. The resonance Raman spectra of Fe_4S_4 model compounds have proven to be sensitive indicators of small changes in cluster geometry, with the conversion from T_d to D_{2d} geometry being accompanied by the expected increase in the total number of Fe–S stretching modes.[13] Further distortions leading to geometries lower than D_{2d} are certainly a possibility but would require a greater number of Fe–S^b modes[26] than can be detected at the present level of resolution. The RR spectrum of oxidized ferredoxin from *C. pasteurianum* closely matches that of the D_{2d}-distorted model complex $(Et_4N)_2[Fe_4S_4(SCH_2Ph)_4]$ in both the number and the relative intensities of the vibrational modes.[13,26] This information, combined with normal coordinate analysis and sulfur isotope dependence, has led to the complete assignment of the RR spectrum of *Cp* Fd (Figure 1a and Table I). A set of 10 Fe–S stretching modes is associated with the $Fe_4S_4(Cys)_4$ chromophore. The spectrum is dominated by a strong band at 338 cm^{-1}, which arises from the totally symmetric stretch of the Fe_4S_4 core. A five-band pattern at lower energy is due to additional vibrations of the bridging sulfides. Another set of four bands at higher energy is attributed mainly to terminal Fe–S(Cys) modes. Altogether, the RR spectra provide convincing evidence for D_{2d} or lower symmetry in the $Fe_4S_4(Cys)_4$ clusters of *Cp* Fd.

The resonance Raman spectrum of ferredoxin from *C. acidi-urici* (Figure 1b) is almost identical with that of *Cp* Fd and is again characteristic of an $Fe_4S_4(Cys)_4$ cluster with a D_{2d} distortion. On the basis of amino acid sequence homologies of 70–75%, *Cp* and *Ca* Fds are closely related to one another and to *Pa* Fd.[27] A low-resolution structure of *Ca* Fd[28] suggests the same polypeptide chain folding as in *Pa* Fd. The high-resolution crystal structures of the most distantly related ferredoxins from *A. vinelandii* (*Av*) and *B. thermoproteolyticus* (*Bt*) also show Fe–S bond distances and bond angles similar to *Pa* Fd.[11b] It is likely that a distorted $Fe_4S_4(Cys)_4$ cluster geometry is common to all ferredoxins. However, the extent of the deformation is small and is more readily detected by Raman spectroscopy than by X-ray crystallography.

(b) High-Potential Iron Proteins. The RR spectra of reduced HiPIPs are indicative of a similar type of tetragonal distortion of the $Fe_4S_4(Cys)_4$ cluster. The RR spectrum of *R. globiformis* $HiPIP_{red}$ (Figure 1c) has essentially a peak-for-peak correspondence with the RR spectra of *Cp* and *Ca* ferredoxins. A comparison of reduced HiPIPs from four different organisms

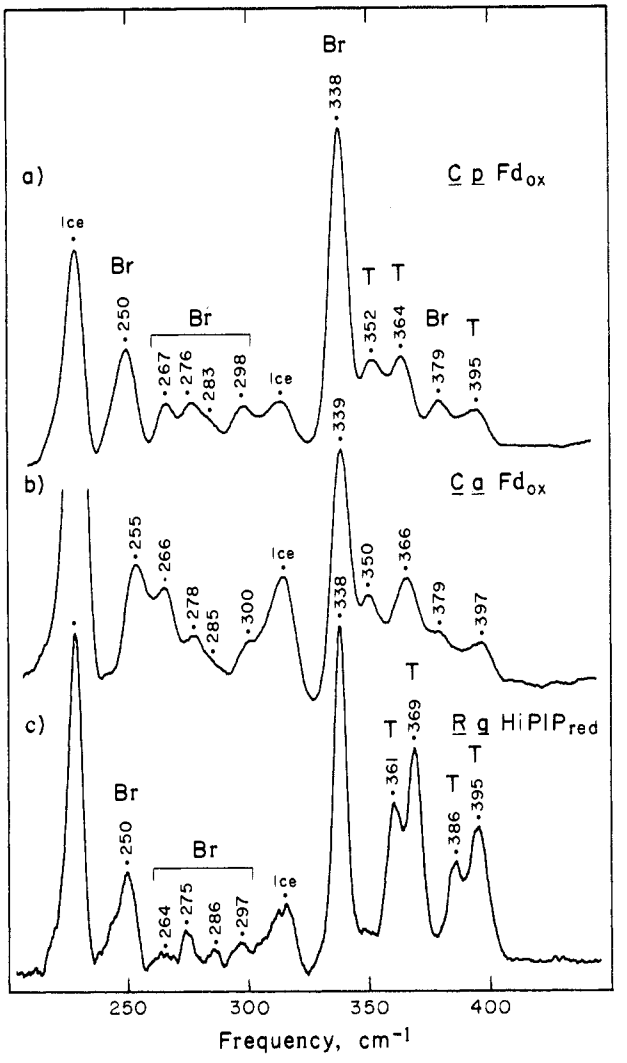

Figure 1. RR spectra of (a) Fd_{ox} from *C. pasteuranium*, (b) Fd_{ox} from *C. acidi-urici*, and (c) $HiPIP_{red}$ from *R. globiformis*. *Cp* Fd and *Cv* Fd (~2 mM) were in 0.05 M Tris–0.1 M NaCl (pH 8.0); *Rg* HiPIP (~1 mM) was in 0.1 M phosphate (pH 7.0). Spectrum a was recorded at 15 K with 488.0-nm excitation (160 mW), 6-cm^{-1} spectral resolution, scan rate of 1 cm^{-1}/s, and 40 scans. Spectra b and c were recorded under similar conditions, but with 476.5-nm excitation (100 mW) for (b) and 488.0-nm excitation (250 mW), 5-cm^{-1} spectral resolution, 10 scans for (c). T refers to terminal Fe–S^t(Cys) mode, and Br refers to bridging Fe–S^b mode as assigned in Table I.

(25) Carter, C. W., Jr. *J. Biol. Chem.* **1977**, *252*, 7802–7811.
(26) Moulis, J.-M.; Meyer, J.; Lutz, M. *Biochemistry* **1984**, *23*, 6605–6613.
(27) (a) Otaka, E.; Ooi, T. *J. Mol. Evol.* **1987**, *26*, 257–267. (b) Fitch, W. M.; Bruschi, M. *Mol. Biol. Evol.* **1987**, *4*, 381–394.
(28) Krishna Murthy, H. M.; Hendrickson, W. A.; Orme-Johnson, W. H.; Merritt, E. A.; Phizackerley, R. P. *J. Biol. Chem.* **1988**, *263*, 18430–18436.

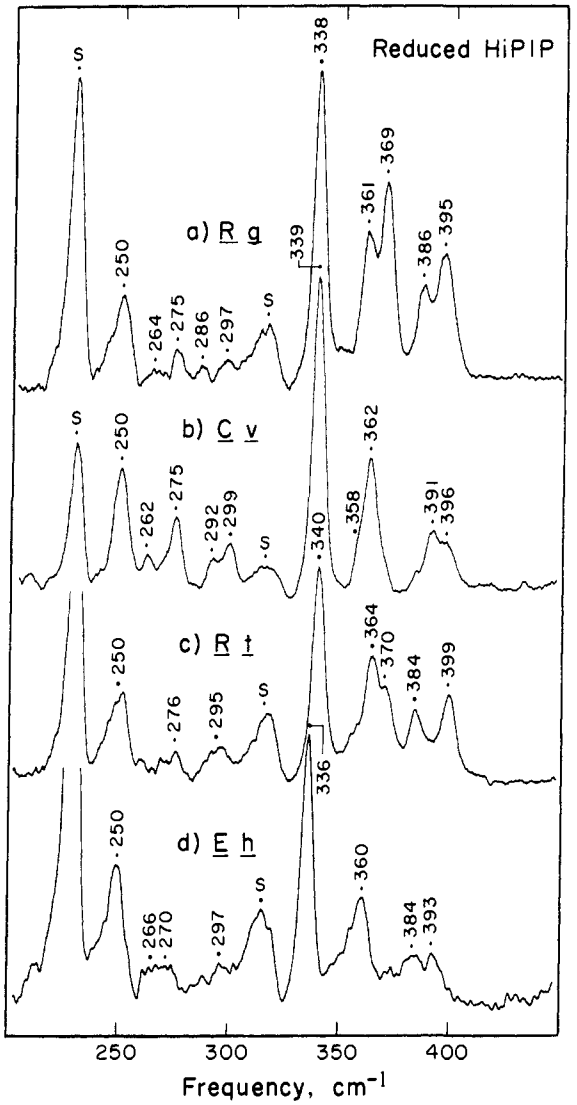

Figure 2. RR spectra of reduced HiPIPs from (a) *R. globiformis*, (b) *C. vinosum*, (c) *R. tenuis*, and (d) *E. halophila*. Proteins (~1 mM) were in 0.1 M phosphate (pH 7.0). Samples for (c) and (d) were reduced with 5 mM dithionite. Spectral conditions as in Figure 1c except for *Cv* HiPIP, which was at 1.5 mM and 20 scans. S denotes peaks from frozen solvent.

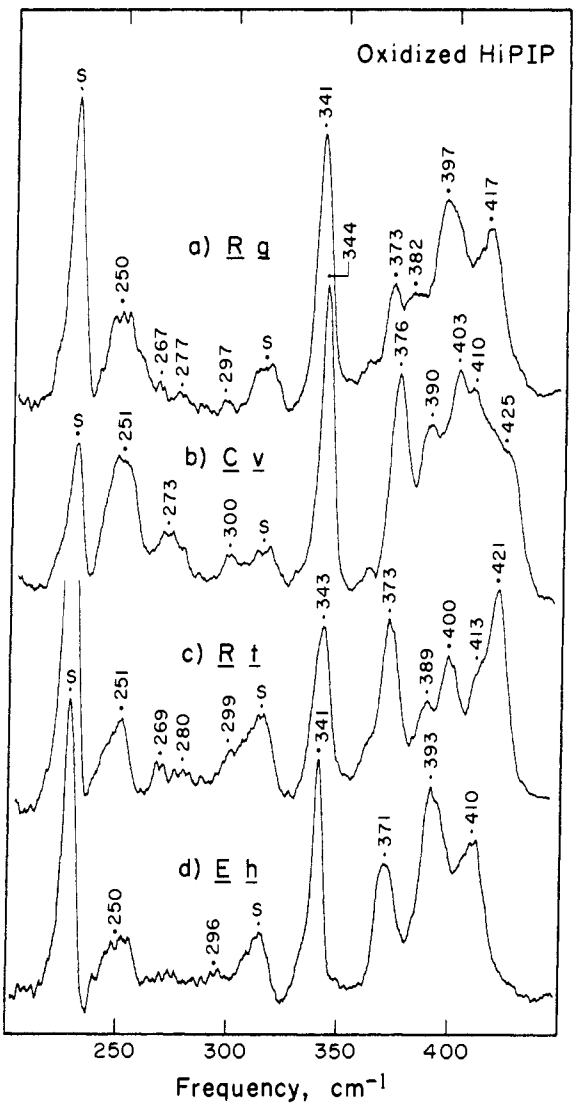

Figure 3. RR spectra of oxidized HiPIPs from (a) *R. globiformis*, (b) *C. vinosum*, (c) *R. tenuis*, and (d) *E. halophila*. Proteins (~1 mM) were in 0.1 M phosphate (pH 7.0). Samples for (a–c) were oxidized with $K_3Fe(CN)_6$ at concentrations of 10, 10, and 2 mM, respectively. Spectral conditions as in Figure 1c.

reveals the 9–10-band pattern typical of D_{2d}-distorted clusters (Figure 2). The appropriateness of the D_{2d} description for the tetranuclear cluster in HiPIP had been questioned earlier on the basis that the four RR peaks above 350 cm^{-1} in *Cp* Fd appeared to be merged into two broad peaks in *Cv* HiPIP, an occurrence more characteristic of T_d symmetry.[13] However, the higher resolution of the present RR spectrum for *Cv* HiPIP (Figure 2b), as well as the appearance of four well-resolved modes above 350 cm^{-1} in the RR spectra of *Rg* and *Rt* HiPIPs (Figure 2a,c) make the lowered symmetry of these clusters a certainty. Moulis et al.[26] reached a similar conclusion regarding the applicability of D_{2d} symmetry for the iron cluster of *Cv* HiPIP on the basis of their high-quality RR spectrum.

Oxidation of *Cv* HiPIP to the $[Fe_4S_4(Cys)_4]^{1-}$ state is accompanied by an ~0.1-Å contraction in the overall size of the cluster as expected for the increase in iron charge.[7a] Since the eight long Fe–S^b bonds in reduced HiPIP appeared to undergo the greatest shortening, it was suggested that the oxidized Fe_4S_4 core adopts a more nearly tetrahedral symmetry. However, the RR spectrum for oxidized *Cv* HiPIP (Figure 3b) gives no indication of an increase in symmetry. A comparison of the oxidized HiPIPs from the four different organisms shows that their RR spectra are remarkably similar (Figure 3) and also resemble those of the reduced forms. The spectra are again dominated by the totally symmetric vibration of the Fe_4S_4 core near 343 cm^{-1}, whose 3–5-cm^{-1} upshift (relative to the value for the reduced protein) is expected from the overall shortening of Fe–S^b bonds. There are three to four Fe–S^b modes to lower energy, which are more difficult to quantitate because of their diminished intensity. The predominately Fe–S(Cys) modes to higher energy have increased to five or six in number; two new vibrations are above 400 cm^{-1}, and this region shows markedly enhanced intensities. On the basis of the observation of nine or more stretching modes in the RR spectra of oxidized HiPIPs, a symmetry lower than T_d must still be postulated.

The HiPIPs used in this study were chosen, in part, for their wide range in redox potentials: *Rg* (+450 mV), *Cv* (+360 mV), *Rt* (+330 mV), and *Eh* (+120 mV).[5] The fact that their resonance Raman spectra are so similar indicates that the $Fe_4S_4(Cys)_4$ clusters in these four HiPIPs have nearly identical geometries. Thus, the ~350-mV range in redox potentials must be due to differences in the environments of these clusters within the proteins.

Raman Spectral Assignments for Fd and HiPIP. Vibrational assignments for oxidized *Cp* ferredoxin have been given by Czernuszewicz et al.[13] based on ^{34}S substitution, normal coordinate analysis for D_{2d} symmetry, and comparison with model complexes (Table I). The designation of a set of six bridging Fe–S^b modes between 250 and 340 cm^{-1}, one Fe–S^b mode near 380 cm^{-1}, and two terminal Fe–S(Cys) modes between 350 and 365 cm^{-1} (Figure

Table II. Fe–S_γ–C_β–C_α Dihedral Angles in Rubredoxin, Ferredoxins, and HiPIP[a]

$Fe(Cys)_4$ in Rd_{ox}[b]	$Fe_2S_2(Cys)_4$ in Fd_{ox}[b]	$Fe_4S_4(Cys)_4$ in Fd_{ox}[c] cluster I	$Fe_4S_4(Cys)_4$ in Fd_{ox}[c] cluster II	$Fe_4S_4(Cys)_4$ in HiPIP red[d]	$Fe_4S_4(Cys)_4$ in HiPIP ox[b]
188 (39)	199 (49)	62 (8)	61 (36)	123 (63)	128 (63)
193 (6)	244 (46)	86 (46)	84 (18)	180 (46)	198 (46)
269 (9)	260 (79)	244 (14)	252 (42)	274 (77)	270 (77)
273 (42)	285 (41)	302 (11)	298 (39)	293 (43)	285 (43)

[a] Dihedral angle in degrees (residue number in parentheses). [b] Data for rubredoxin from *Clostridium pasteurianum*, ferredoxin from *Spirulina platensis*, and *Cv* HiPIP taken from ref 35 and based on Brookhaven Data Bank coordinates for 5RXN, 3FXC, and 1HIP, respectively. [c] From the refined structure of *Pa* Fd (this work). [d] From coordinates provided by Dr. C. W. Carter, Jr., for refined structure of *Cv* $HiPIP_{red}$ at 2.0-Å resolution.

1a) is in general agreement with the earlier assignments of Moulis et al.[26] based on ^{34}S and Se substitutions. Only the assignment of the 395-cm^{-1} peak as a terminal Fe–S(Cys) mode remains somewhat in question owing to a greater bridging ^{34}S shift in the proteins than in the model complexes.

The close matching of the RR spectra of Fd_{ox} and $HiPIP_{red}$ (Figure 1) implies similar vibrational assignments for the two proteins. In addition, selenium-substituted *Cp* Fd_{ox} and *Cv* $HiPIP_{red}$ with $[Fe_4Se_4]^{2+}$ cores have closely matched RR spectra.[26,29] For *Cp* Fd, all seven of the modes assigned to bridging vibrations (Table I) shift to lower energy in the Fe_4Se_4 protein.[26] For *Cv* HiPIP, the same Se-dependent shifts are observed for the six peaks between 250 and 340 cm^{-1}, leading them to be assigned to the same Fe–S^b vibrations as in Fd.[29] In contrast, the four peaks between 358 and 396 cm^{-1} in *Cv* $HiPIP_{red}$ are relatively unaffected by selenium substitution,[29] suggesting that they may all be Fe–S^t modes. Four of the five peaks between 376 and 425 cm^{-1} in *Cv* $HiPIP_{ox}$ (Table I) are similarly unaffected when the bridging sulfido groups are replaced by seleno groups.[29]

The above data indicate that HiPIPs may have as many as four Fe–S(Cys) vibrations, when a maximum of three is expected for D_{2d} symmetry. It is possible that the multiplicity of RR peaks in *Cv* $HiPIP_{ox}$ is due to a mixture of protein conformations, but it would be remarkable for the proteins from four different species (Figure 3) to all have a similar mixture of conformations. Moreover, NMR spectra of various HiPIPs give no such indication of multiple conformers.[18b,30] Moulis et al.[29] have also suggested that the higher vibrational frequencies near 420 cm^{-1} for ν(Fe–S^t) in *Cv* $HiPIP_{ox}$ could be due to a differential shortening of particular Fe–S(Cys) bonds. The decrease in Fe–S bond lengths in $HiPIP_{ox}$ predicted from the higher RR frequencies is actually contrary to the X-ray data, where the variation in Fe–S(Cys) distances is 2.16–2.22 Å in $HiPIP_{red}$ and 2.18–2.26 Å in $HiPIP_{ox}$ (based on coordinates from C. W. Carter, Jr.).

A preferable explanation for both the larger number and higher energy of Fe–S(Cys) modes in HiPIP relates to the conformations of the cysteine ligands. The RR spectra of the $Fe(Cys)_4$ rubredoxins and the Fe_2S_2 ferredoxins show unexpected splittings and unusually high frequencies for the ν(Fe–S^t) modes above 320 cm^{-1}.[31] Both of these effects have been ascribed to coupling of Fe–S(Cys) stretching modes with the cysteine S–C–C deformation near 300 cm^{-1}. Such coupling is expected to be strongly dependent on the Fe–S_γ–C_β–C_α dihedral angle, being minimal at 90° and maximal at 180°.[31b] The actual distribution of Fe–S_γ–C_β–C_α angles in rubredoxin is two near 180° and two near −90°, whereas Fe_2S_2 ferredoxin has one near 180° and three near −90° (Table II). Thus, both proteins have at least one cysteine residue capable of coupling ν(Fe–S^t) with δ(S–C–C).

Table III. Comparison of Amide Hydrogen Bonds[a] to $Fe_4S_4(Cys)_4$ Clusters in Ferredoxin and HiPIP

Bt Fd_{ox}[b] cluster I		*Pa* Fd_{ox}[c] cluster I		*Pa* Fd_{ox}[c] cluster II		$HiPIP_{red}$[d]	
NH···S	Å	NH···S	Å	NH···S	Å	NH···S	Å
large loop							
12 S*2	3.8	9 S*2	3.3	37 S*1	3.5	77 S*1	3.5
13 γ11	3.5	10 γ8	3.4	38 γ36	3.6	79 γ77	3.4
15 S*1	3.4	12 S*1	3.4	40 S*4	3.4	81 γ46	3.6
16 γ14	3.6	13 γ11	3.4	41 γ39	3.5		
17 S*4	3.4	14 S*4	3.5	42 S*3	3.4		
small loop							
63 γ61	3.8	48 γ46	3.4	20 γ18	3.9	48 γ46	3.5
65 γ61	3.1	50 γ46	3.4	22 γ18	3.4	49 S*2	*e*
extra site							
33 γ11	3.7	29 γ8	3.4	2 γ36	3.5	65 γ63	3.4

[a] Reported distance in angstroms (±0.2 Å) is between amide nitrogen and bridging (S*) or terminal (γ) sulfur. The NH···S bonds were identified by distances of 3.9 Å or less and angles of 120° or more, as have been observed in small compounds (ref 35). NH···S bonds are considerably weaker than NH···O bonds.[15,36] [b] Data for *B. thermoproteolyticus* Fd from ref 11b. [c] From present structure refinement. [d] From ref 17. [e] The 3.9-Å hydrogen bond reported previously[17] is unlikely because of its unfavorable angle of <100° and its considerable length.

The angular parameters for *Cv* HiPIP (Table II) are similar to rubredoxin and Fe_2S_2 ferredoxin in having at least one Fe–S_γ–C_β–C_α dihedral angle near 180°, in addition to one at ~125° and two near −90°. In contrast, the $Fe_4S_4(Cys)_4$ clusters in *Pa* Fd have two Fe–S_γ–C_β–C_α angles nearer +90° and two nearer −90°. This difference would explain why the RR spectra of $HiPIP_{red}$ and $HiPIP_{ox}$ show an *increased number* of Fe–S(Cys) modes, whereas the RR spectrum of Fd_{ox} is closer to that of the $(Et_4N)_2[Fe_4S_4(SCH_2Ph)_4]$ complex[13] whose Fe–S–C–C angles are also near 90°.[32] The *higher frequencies* for the Fe–S(Cys) modes in HiPIP, particularly in the oxidized state, are also consistent with increased coupling of ν(Fe–S^t) and δ(S–C–C). Han et al.[31b] have shown that the frequencies of Fe–S(Cys) modes above 300 cm^{-1} are expected to increase as the dihedral angle changes from 90° to 180°.

Hydrogen Bonds in Crystal Structures of Ferredoxins. The structure of *Pa* Fd was originally refined against 2.0-Å data by using alternating differential difference Fourier and idealization methods available at the time.[8b] The *R* value reached 0.188 for a model that included 146 solvent positions in addition to the protein atoms. That publication also reported a perceived discrepancy in the chemical identity of residue 23 (Ile vs Gln for an internal residue) and noted difficulty at a turn between residues 26 and 28. Using better graphics[33] and refinement programs,[24] we have now refined the model to an *R* of 0.137 with 86 solvent positions. A difference density map with the earlier coordinates and no solvent included showed a large positive peak associated with residue 22 (ostensibly Ile) and a large shift peak near the troublesome bend. Replacing 22 with a Cys, and inserting a residue (Gln) after residue 24, ameliorates both problems. Whereas, the previous X-ray sequence starting at residue 18 was CPVNIIQG, and the previous chemical sequence was CPVNIQQG, the current X-ray sequence is CPVNCIQQG. The new Cys 22 fills a gap in the sequence alignment with other clostridial-type ferredoxins[27b] and has been confirmed by chemical sequencing.[34] Thus, the number of all residues beyond 22 must

(29) Moulis, J.-M.; Lutz, M.; Gaillard, J.; Noodleman, L. *Biochemistry* **1988**, *27*, 8712–8719.
(30) Sola, M.; Cowan, J. A.; Gray, H. B. *J. Am. Chem. Soc.* **1989**, *111*, 6627–6630.
(31) (a) Czernuszewicz, R. S.; LeGall, J.; Moura, I.; Spiro, T. G. *Inorg. Chem.* **1986**, *25*, 696–700. (b) Han, S.; Czernuszewicz, R. S.; Kimura, T.; Adams, M. W. W.; Spiro, T. G. *J. Am. Chem. Soc.* **1989**, *111*, 3505–3511.
(32) Averill, B. A.; Herskovitz, T.; Holm, R. H.; Ibers, J. A. *J. Am. Chem. Soc.* **1973**, *95*, 3523–3534.
(33) (a) Jones, T. A. *J. Appl. Crystallogr.* **1978**, *11*, 268–272. (b) CCP4 (1979), S.E.R.C. Collaborative Computing Project No. 4, A suite of Programs for Protein Crystallography; Daresbury Laboratory, Warington WA4 4AD, United Kingdom.
(34) Adman, E. T.; Sieker, L. C.; Le Trong, H., unpublished results.
(35) Elcombe, M. M.; Taylor, J. C. *Acta Crystallogr.* **1968**, *A24*, 410–418.
(36) (a) Pimentel, G. C.; McClellan, A. L. *Annu. Rev. Phys. Chem.* **1971**, *22*, 347–385. (b) Pogorely, V. K. *Russ. Chem. Rev.* (*Engl. Transl.*) **1977**, *46*, 316–336.

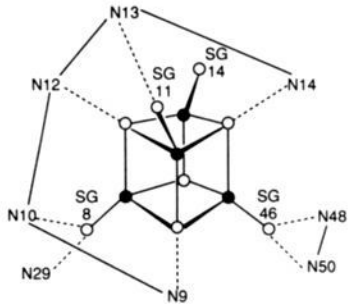

Fd_{ox} Cluster I

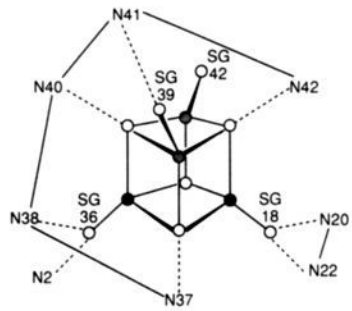

Fd_{ox} Cluster II

Figure 4. Schematic drawing of clusters I and II of *Pa* ferredoxin. Iron atoms (●), sulfur atoms (○), and hydrogen bonds (- -). Thin lines denote backbone connection of nearby hydrogen-bonding amide groups in the polypeptide chain. N stands for amide and SG for γ-sulfur of cysteine.

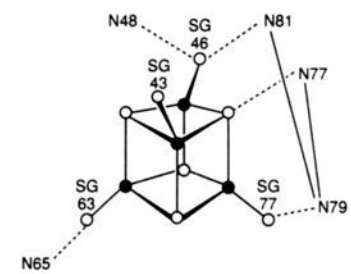

$HiPIP_{red}$

Figure 5. Schematic drawing of Fe_4S_4 cluster in reduced *Cv* HiPIP based on Sheridan et al.[17] Symbols as in Figure 4.

now be increased by one relative to previous reports of the structure of *Pa* Fd.

The two $Fe_4S_4(Cys)_4$ clusters in *Pa* Fd were found to have almost identical structures and protein environments, suggesting a 2-fold symmetry relating the arrangement of the clusters in the protein.[8a] The likelihood that the two cluster sites arose via gene duplication has been well documented by analyses of amino acid sequence homologies.[27b] Three of the cysteine ligands to each cluster are located in a large loop with the sequence, Cys-X_2-Cys-X_2-Cys. The fourth cysteine ligand of each cluster is derived from a separate region of the polypeptide with a common Cys-Pro-Val sequence.

Examination of the newly refined structure of *Pa* Fd reveals even greater similarities between the two clusters (Figure 4). The conformation of the protein backbone in the vicinity of the cluster is highly conserved. The two clusters have an identical set of eight hydrogen bonds between main-chain amide NH groups and terminal or bridging sulfur atoms (Table III and Figure 4). The large Cys-X_2-Cys-X_2-Cys loop (residues 8–14 or 36–42) is stabilized in each case by the same five hydrogen bonds to the same five sulfur atoms, where the amide donor pattern is $(NH)_2$-X-$(NH)_3$. Similarly, the small Cys-Pro-Val loop (residues 46–50 or 18–22) is stabilized by the same two hydrogen bonds to the remaining cysteine sulfur ligand with the amide pattern (NH)-X-(NH). Another indication of the degree of conservation is that each of the cysteine ligands has a Fe–S_γ–C_β–C_α dihedral angle similar to its counterpart in the other cluster (Table II). The S_γ–C_β–C_α–N dihedral angles of 181°/185° (Cys 8/36, 73°/78° (Cys 11/39), 63°/53° (Cys 14/42), and 183°/182° (Cys 46/18) are also conserved for homologous cysteines.

An equally remarkable conservation of $Fe_4S_4(Cys)_4$ cluster structure has been observed for cluster I of *Bt* Fd and cluster II of *Av* Fd. The polypeptide conformations in the large and small loops surrounding each cluster are essentially superimposable on those of *Pa* Fd.[11b] Also the same eight NH···S hydrogen bonds are present: five from the large loop, two from the small loop, and one from the extra site (Table III). The cysteine Fe–S_γ–C_β–C_α dihedral angles are also conserved. For example, *Av* Fd cluster II has dihedral angles[37] of 63°, 69°, 252°, and 296°, which are very close to the values for *Pa* Fd cluster II (Table II). The Fe_3S_4 cluster of ferredoxin from *Desulfovibrio gigas* shows the same protein-folding pattern.[38] There are again five hydrogen bonds from the large loop (amides 9–12 and 14), two from the small loop (amides 52 and 54), and one from the extra site (amide 31). The only differences from *Pa* Fd (Figure 4) are that N13 is no longer hydrogen bonded owing to the absence of the Fe normally coordinated to Cys 11, and the bridging S at the bottom of the cluster is hydrogen bonded to N11 as well as N9.[38] Thus, the protein geometry about the iron–sulfur cluster appears to be highly conserved among at least four of the different classes of ferredoxins: clostridial (*Peptococcus*), *Azotobacter*, *Desulfovibrio*, and *Bacillus*.[11a]

Hydrogen Bonds in Crystal Structures of HiPIPs. The crystal structure of *Cv* HiPIP[7a] shows that the $Fe_4S_4(Cys)_4$ cluster is buried in the center of a relatively spherical protein, whereas in *Pa* Fd the two clusters are situated at the ends of an elongated protein and are closer to the protein–solvent interface.[8] There is *no identifiable homology* in the amino acid sequences[22c] or the three-dimensional structures of the two types of proteins. Yet another Fe_4S_4 cluster has been observed in the flavoprotein trimethylamine dehydrogenase, which bears no protein structure homology to either Fd or HiPIP.[39a] Thus, the occurrence of Fe_4S_4 clusters in these different proteins must be the result of convergent evolution. Carter[25] suggested a possible relationship from the observation of similar protein β-sheets connected to two of the cysteine ligands in Fd and HiPIP. A closer comparison of the polypeptide geometries associated with each Fe–S center makes this unlikely.

As can be seen in Figure 5, the pattern of hydrogen bonds and folding of the polypeptide chain in reduced *Cv* HiPIP is completely different from that in Fd (Figure 4). There is a large Cys-X_2-Cys-X_2 loop (residues 43–48) along one side of the cube that provides only one hydrogen bond. There is a smaller loop of five amino acids (residues 77–81) that provides one cysteine ligand and three hydrogen bonds to another side of the cube. The fourth cysteine ligand and its hydrogen bond (residues 63–65) come from a third region of the molecule. The average hydrogen bond distance of 3.5 Å is similar to the average for *Pa* Fd (Table III), but the total number of hydrogen bonds in *Cv* $HiPIP_{red}$ is only five instead of eight. (*Cv* $HiPIP_{ox}$ has the same number of hydrogen bonds but with a 0.1-Å increase in average hydrogen bond distance.[17]) The dihedral angles for two of the four cysteines are completely different in *Pa* Fd and *Cv* HiPIP (Table II). These are the same two cysteines (63 and 46 in HiPIP) for which a common β-sheet connection had been proposed.[25] Thus, the

(37) Chakrabarti, P. *Biochemistry* **1989**, *28*, 6081–6085.
(38) (a) Kissinger, C. R.; Adman, E. T.; Sieker, L. C.; Jensen, L. H.; Legall, J. *FEBS Lett.* **1989**, *244*, 447–450. (b) Kissinger, C. R.; Adman, E. T., unpublished results.
(39) (a) Lim, L. W.; Shamala, N.; Mathews, F. S.; Steenkamp, D. J.; Hamlin, R.; Xuong, N. H. *J. Biol. Chem.* **1986**, *261*, 15140–15146. (b) Adman, E. T.; Sieker, L. C.; Jensen, L. H.; Bruschi, M.; LeGall, J. *J. Mol. Biol.* **1977**, *112*, 113–120. (c) Frey, M.; Sieker, L. C.; Payan, F.; Haser, R.; Bruschi, M.; Pepe, G.; LeGall, J. *J. Mol. Biol.* **1987**, *197*, 525–541.

$Fe_4S_4(Cys)_4$ clusters in Fd and HiPIP exhibit the diversity of polypeptide conformations and protein environments expected of unrelated proteins.

Cysteine ligands in metalloproteins show several common motifs. One is that a given Cys (at position *n*) tends to be present in a chelating loop containing a second Cys ligand (at position *n* + 3) yielding the sequence Cys-X-X-Cys. This pattern is seen in *Cp* rubredoxin (Cys 6/Cys 9, Cys 39/Cys 42) and *Spirulina platensis* (*Sp*) ferredoxin (Cys 46/Cys 49) as well as in *Pa* Fd and *Cv* HiPIP (Table II). Another common feature of cysteine ligands (at position *n*) is that their sulfur atoms are hydrogen bonded to the amide NH of the second residue down the polypeptide chain (at position *n* + 2). Such S···NH bonds are observed for *Cp* rubredoxin (C6···8NH, C9···11NH, C42···44NH)[39b,c] and *Sp* ferredoxin (C41···43NH, C46···48NH)[19] as well as in *Pa* Fd (Cys 8, 11, and 46) and *Cv* HiPIP (Cys 46, 63, and 77) (Table III). Although one might expect the *n* + 2 hydrogen bond and the *n* + 3 cysteine to have the effect of restricting the conformation of the cysteine at position *n*, this does not appear to be the case. The Fe–S_γ–C_β–C_α dihedral angles for such position *n* cysteines vary considerably. For example, *Cp* rubredoxin has dihedral angles of 193° (Cys 6) and 188° (Cys 39), whereas *Pa* ferredoxin has dihedral angles of 62° (Cys 8) and 302° (Cys 11). Additional protein-folding constraints must be involved in stabilizing the particular cysteine conformations that are highly conserved within each class of iron–sulfur protein.

Detection of Hydrogen Bonding by Raman Spectroscopy. Hydrogen bonding to a metal-coordinated ligand, such as oxygen or sulfur, generally results in a decrease in the M–L stretching frequency due to the electrostatic interactions associated with hydrogen bonding. In the case of the dinuclear iron protein hemerythrin, for example, hydrogen bonding to the μ-oxo group causes the ν_s(Fe–O–Fe) mode to undergo a 20-cm^{-1} downshift from ~510 to ~490 cm^{-1}.[40] More subtle changes are observed upon substitution of D for H when the two isotopes have different hydrogen bond strengths. Whether stronger hydrogen bonds are formed with H or with D depends on the specific system being studied.[41] For example, in a crystal structure determination of thiourea and deuterated thiourea by neutron diffraction, the hydrogen-bonded N···S distance varied from 3.35 to 3.91 Å and the difference in N···S distance with D vs H varied from +0.07 Å to −0.04 Å (with a standard deviation of ±0.01 Å).[35] Thus, D substitution can lead to either an increase or a decrease in the M–L stretching frequency. For oxyhemerythrin, hydrogen bonding is stronger with H donors than D donors, and thus, ν_s(Fe–O–Fe) is observed to increase by 4 cm^{-1} (i.e., undergo a smaller decrease) with deuterium.[40] For the blue copper and $Fe_2S_2(Cys)_4$ proteins, hydrogen bonding of amide NH groups to the sulfur ligands results in ν(M–S) decreases of 0.2–2 cm^{-1} with deuterium.[19] The downshifts in the latter two cases are indicative of the amide ND groups forming stronger hydrogen bonds than their NH counterparts; the smaller magnitude of the isotope shifts is consistent with the fact that hydrogen bonds to sulfur are weaker than hydrogen bonds to oxygen,[36] with N···S distances as long as 3.9 Å being observed in model compounds.[35]

The D-exchange rates for amide NH groups in proteins vary considerably, and it may take days to weeks for protons that are hydrogen bonded and buried in a hydrophobic environment to exchange with solvent protons.[42] In their electron spin echo studies of HiPIPs from *Rhodocyclus gelatinosus* (formerly *Rhodopseudomonas gelatinosa*) and *C. vinosum*, Orme-Johnson et al.[14] found no evidence for the exchange of protons in the vicinity of the Fe_4S_4 cluster after several days of incubation in D_2O. However, exchange was achieved by partially unfolding the protein in 80% DMSO. In contrast, the more exposed clusters in *Cp* ferredoxin underwent significant D exchange within 24 h without denaturation. We also found that incubation of *Cv* $HiPIP_{ox}$ for up to 7 days in D_2O under nondenaturing conditions gave no indication of D exchange as measured by RR spectroscopy. Thus, to obtain D-substituted samples of *Cv* HiPIP for our Raman studies, we used the DMSO unfolding/refolding procedure. In addition, we exposed *Cp* and *Ca* apoferredoxins to D_2O or H_2O prior to reconstitution of the cluster in order to be certain of complete isotope exchange for the ferredoxin samples.

Table IV. Deuterium Isotope Shifts in Raman Spectra of Ferredoxins and HiPIPs[a]

Cp Fd_{ox}	*Ca* Fd_{ox}	*Cv* $HiPIP_{red}$	*Cv* $HiPIP_{ox}$	assgnmnt[b]
250	255 (−1)	250	251	Br
267	266	262	273	Br
276 (−1)	278 (−1)	275		Br
283	285	292		Br
298	300	299	300	Br
338	339	339	344	Br
352 (−1)	350 (−1)	358	376 (−1)	T
364 (−1)	366 (−3)	362 (−2)	390 (−1)	T
379 (+2)	379 (+4)			Br
		391 (−1)	403 (−2)	T
395 (−1)	397 (−1)	396 (−1)	417 (−5)	T
			425 (−4)	T

[a] $\Delta\nu$ for D_2O minus H_2O given in parentheses. Raman spectral conditions as in Figures 6 and 7. Isotope shifts are averages of two or three separate experiments and are accurate to ±0.7 cm^{-1}. [b] From Table I.

(a) Ferredoxins. Deuterium substitution in the Fe_4S_4 ferredoxins results in small spectral shifts (Table IV) of a magnitude similar to those observed previously for the $Fe_2S_2(Cys)_4$ ferredoxins.[19] The ferredoxins from *Cp* and *Ca* show a remarkably similar pattern of deuterium isotope shifts (Table IV, Figure 6), implying a conservation of the hydrogen bonds in the four clusters of the two proteins. The three peaks assigned to Fe–S^t modes all shift by −1 to −3 cm^{-1} in D_2O, due to the five hydrogen bonds from the polypeptide backbone to the cysteine sulfur atoms of each cluster (Figure 4). The majority of the Fe–S^b modes between 250 and 338 cm^{-1}, including the totally symmetric vibration at 338 cm^{-1}, have no detectable D dependence despite the likelihood of three hydrogen bonds to bridging sulfur atoms. The only consistent changes are in the Fe–S^b modes at 276 (−1-cm^{-1} shift in D_2O) and 379 cm^{-1} (+2- to +4-cm^{-1} shift in D_2O). The hydrogen bonds that contribute to the 276-cm^{-1} vibration are apparently stronger in D_2O, whereas those affecting the 379-cm^{-1} vibration are apparently stronger in H_2O. These opposing forces could explain the failure to observe D effects on the other Fe–S^b modes.

The deuterium isotope shifts shown in Figure 6 were obtained from Fd samples where the apoprotein was equilibrated with H_2O or D_2O prior to reconstitution of the iron–sulfur cluster. Similar deuterium isotope shifts were observed after exposing *native Cp* and *Ca* ferredoxins to D_2O for 18 h, but this was accompanied by some oxidation of the cluster. These results show that the H-bonding amide groups in Fds are accessible to solvent even when the clusters remain intact inside the protein and suggest that breathing motion is important in providing solvent access.

(b) High-Potential Iron Proteins. When reduced *Cv* HiPIP in H_2O was subjected to the DMSO procedure for 20 min, the resulting $HiPIP_{red}$ and $HiPIP_{ox}$ samples gave Raman spectra (Figure 7) essentially identical with the untreated proteins (Figures 2 and 3). Extension of the DMSO incubation period to 2 h resulted in a loss of spectral quality. The HiPIP samples in D_2O show a number of isotope shifts in the peaks assigned to Fe–S^t vibrational modes. For *Cv* $HiPIP_{red}$, three of the Fe–S^t modes shift by −1 to −2 cm^{-1} in D_2O (Table IV, Figure 7). The fourth mode at ~358 cm^{-1} is too weak to determine its location with certainty. The D sensitivity of the Fe–S(Cys) stretching modes is in the same direction and of the same magnitude as in *Cp* and *Ca* Fd. This is in agreement with the similarity in the number and strength of the hydrogen bonds (four for HiPIP and five for Fd) to terminal sulfur ligands (Table III). In contrast, none of the Fe–S^b modes in *Cv* $HiPIP_{red}$ show any indication of deuterium dependence. This is consistent with the markedly smaller number

(40) Shiemke, A. K.; Loehr, T. M.; Sanders-Loehr, J. *J. Am. Chem. Soc.* **1986**, *108*, 2437–2443.
(41) Buckingham, A. D.; Fan-Chen, L. *Int. Rev. Phys. Chem.* **1981**, *1*, 253–269.
(42) (a) Wüthrich, K.; Wagner, G. *Trends Biochem. Sci.* **1984**, *9*, 152–154. (b) Creighton, T. E. *Proteins: Structures and Molecular Principles*; W. H. Freeman: New York, 1984; pp 277–284.

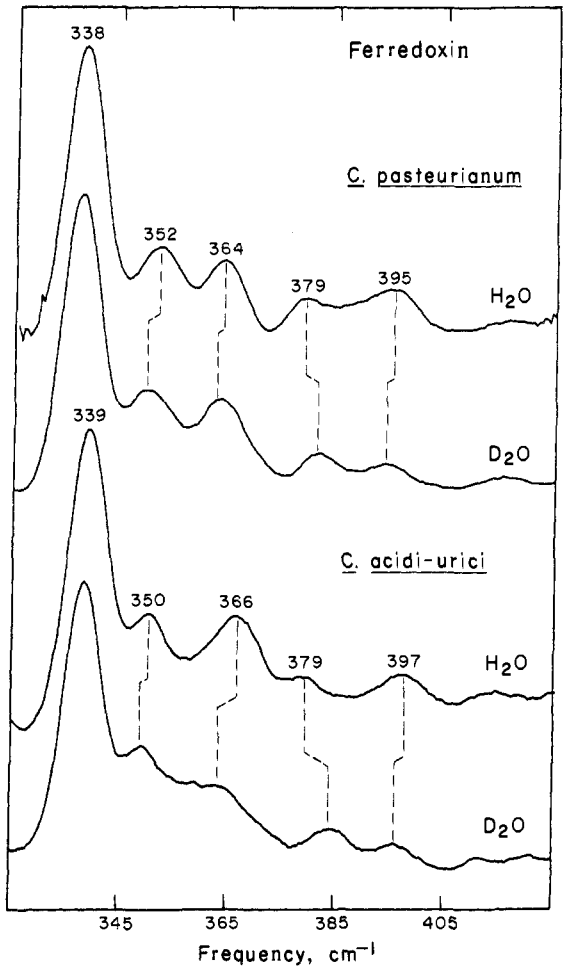

Figure 6. RR spectra of oxidized ferredoxins from *C. pasteurianum* and *C. acidi-urici* in H_2O and D_2O. *Cp* Fd (4 mM) and *Ca* Fd (2 mM) in 0.05 M Tris–0.1 M NaCl (pH 8.0) were prepared by reconstitution of the apoprotein in H_2O or D_2O. Spectral conditions as in Figure 1a (*Cp* Fd) and 1b (*Ca* Fd) with a total of 28, 43, 62, and 54 scans, respectively.

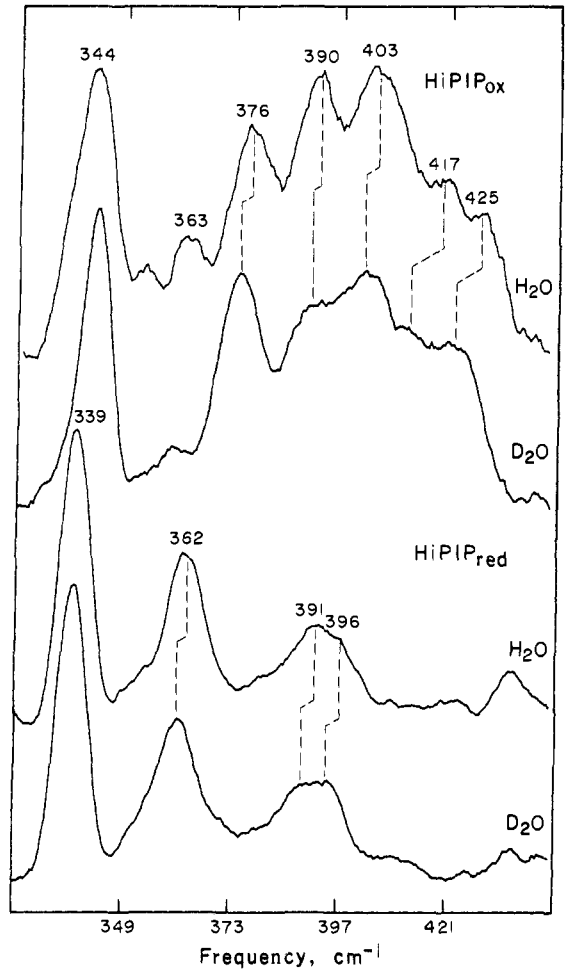

Figure 7. RR spectra of oxidized and reduced *Cv* HiPIP in H_2O and D_2O. Samples ~3 mM in protein in 0.05 M phosphate (pH reading 7.5) underwent isotope exchange by being partially unfolded in 80% DMSO for 20 min. Spectral conditions as in Figure 1c except for 60 mW ($HiPIP_{ox}$) and 150 mW ($HiPIP_{red}$) with a total of 10, 20, 40, and 20 scans, respectively. Spectrum of $HiPIP_{ox}$ in H_2O has shoulder at 339 cm^{-1} and peak at 363 cm^{-1} due to residual reduced protein.

Table V. Redox Potentials of $Fe_4S_4(SR)_4$ Clusters in Proteins and Model Compounds[a]

$Fe_4S_4(SR)_4$ sample	cluster charge 1−/2−	cluster charge 2−/3−
ferredoxin		
B. stearothermophilus[b]		−280
C. pasteurianum[c]		−390
P. aerogenes[c]		−427
C. acidi-urici[c]		−434
A. vinelandii[d]		−645
high-potential iron protein		
R. globiformis[e]	+450	
C. vinosum[e]	+360	
R. tenuis[e]	+330	
E. halophila[e]	+120	
model compound (SR ligand)		
SCH_2CH_2OH in H_2O[f]		−750
SCH_2CH_2OH in DMSO[f]		−1,170
S-2,4,6-(*i*-Pr)$_3C_6H_2$[g]	−120	−1,200

[a] E_m in millivolts, determined between pH 7 and 8.5 vs SHE for proteins and vs SCE for models. [b] Reference 2. [c] Reference 4. [d] Reference 43. [e] Reference 5. [f] Reference 49a. [g] In CH_2Cl_2.[50]

of hydrogen bonds to bridging sulfurs (one for HiPIP and three for Fd, Table III).

Oxidized *Cv* HiPIP exhibits D isotope effects similar to those of reduced *Cv* HiPIP (Table IV, Figure 7). The Fe–S^b modes are again devoid of any D sensitivity. Each of the five peaks assigned to Fe–S^t modes (Table I) shifts by −1 to −5 cm^{-1} in D_2O. Oxidized iron–sulfur clusters are expected to have weaker hydrogen bonds and, thus, a smaller D isotope dependence.[19] The larger isotope shifts associated with *Cv* $HiPIP_{ox}$ are probably a consequence of the greater coupling of Fe–S^t stretches with the cysteine S–C–C deformation. It is of interest that Cys 46, which has been implicated in this coupling by virtue of its Fe–S_γ–C_β–C_α dihedral angle being close to 180° (Table II), is also involved in two hydrogen bonds (Figure 5). No such D effects were observed for HiPIP that had been incubated in D_2O for 7 days without unfolding. This demonstrates that the amide groups that hydrogen bond to the cysteine sulfurs are not accessible to solvent in the native protein.

Redox Potentials of Ferredoxins. Despite the fact that the ferredoxins appear to have totally conserved structures in the vicinity of their Fe_4S_4 clusters, they exhibit a range of redox potentials spanning more than 350 mV (Table V). Clusters I and II in *Cp*, *Pa*, and *Ca* Fds have essentially indistinguishable potentials near −400 mV. Cluster I in *Bt* Fd may have a potential closer to −300 mV since the protein sequence for *Bt* Fd differs from that of *Bacillus stearothermophilus* Fd by only two Asp/Glu interchanges.[11a] Cluster II of *Av* Fd has a redox potential of −640 mV (pH 7.4),[43] similar to the four-iron cluster of *Azotobacter chroococcum* Fd.[4b]

An ~400-mV range in redox potential has also been observed for HiPIPs, which vary from +450 to +50 mV, and for cytochromes *c*, which vary from +470 to +30 mV.[5] The variation

(43) Armstrong, F. A.; Burgess, B. K., personal communication.

in redox potentials of the cytochromes *c* parallels that of the Fds since in both series the protein structure around the metal site is highly conserved. One factor contributing to these variable redox potentials is the local electrostatic environment in the vicinity of the metal center.[44] For example, removal of an internal positive charge in cytochrome *c*[45] or addition of an internal negative charge in myoglobin[46] causes a 50–200 mV drop in redox potential. An even greater drop of 300–450 mV has been observed upon addition of an extra thiolate ligand to $Fe_4S_4(SR)_4$ clusters.[47] As expected, development of a more negative charge in the vicinity of the redox center stabilizes the oxidized relative to the reduced form. In contrast, making the environment less polar favors the reduced form (net charge of 0) in cytochrome *c*[44c] and the oxidized cluster (net charge of 1−) in HiPIPs.[18b]

The variation in reduction potential between *Bt*, *Pa*, and *Av* ferredoxins must also be due to differences in the local environments of the clusters, rather than differences in hydrogen bonds to the clusters or differences in coordination of the cluster to the protein. The crystal structures of these three ferredoxins show identical polypeptide folding, cysteine dihedral angles, and amide hydrogen bonds to the $Fe_4S_4(Cys)_4$ moiety. These features are so highly conserved as to yield *superimposable* cluster binding loops for *Bt*, *Pa*, and *Av* Fds.[11b] The overall size of *Av* Fd is considerably larger than *Bt* and *Pa* Fds, but the *Av* Fd α-carbons for residues 1–58 (which contain all of the cysteine ligands to the two clusters) have the same folding pattern as the α-carbon backbone of *Pa* Fd.[10] Furthermore, the cluster II region of *Av* Fd is at the same distance from the protein surface as in the other two Fds. Although the refined structure of *Pa* Fd indicates that there are no immobilized water molecules in the vicinity of either cluster, breathing motions must allow intermittent access of solvent to the cluster. The most likely explanations for the unusually low E_0' of *Av* Fd are microenvironmental effects, such as more bulky nonpolar groups, which limit solvent accessibility to the cluster. The charged residues in Fds (other than the sulfur ligands) are all located on the *surface* of the protein and do not appear to have a significant effect on the redox potential. In *Pa* Fd for example, there is a distinct clustering of negative surface charges at one end of the molecule (closer to cluster I),[48] yet the redox potentials of clusters I and II are indistinguishable.

Redox Potentials of HiPIPs. Even greater differences in redox potential occur between Fds and HiPIPs, resulting in the stabilization of two different sets of oxidation states. Yet X-ray crystallography shows similar $Fe_4S_4(Cys)_4$ core structures for these two classes of proteins. In the RR spectra, the near coincidence of vibrational frequencies for both Fe–S^b and Fe–S^t modes indicates comparable ground-state structures, whereas the variability of vibrational intensities suggests small differences in electronic excited-state structures. Thus, the differential redox behavior of HiPIPs and Fds would appear to be determined mainly by protein environmental factors other than cluster geometry.

It has been possible to model the redox behavior of ferredoxins and HiPIPs by using $Fe_4S_4(SR)_4$ complexes that are soluble in both aqueous and organic solvents. Thus, clusters with SR ligand such as SCH_2CH_2OH (dissolved in water at alkaline pH) or SC_6H_4-*p*-C_8H_{17} (in aqueous micelles) have SHE-corrected redox potentials of approximately −510 and −400 mV, respectively.[49] These E_m values are in the range of the ferredoxins. Dissolution of the same clusters in organic solvents results in considerably more negative redox potentials (Table V). Use of a sterically hindered ligand with additional nonpolar isopropyl substituents[50] leads to a further decrease in the E_m of the 2−/3− redox couple in organic solvents and actually favors a shift to the 1−/2− oxidation levels (Table V). Similar results have been obtained with adamatane thiolate and bulkier macrocycles as SR ligands.[51] The achievement of the 1−/2− redox couple reproduces the redox levels in HiPIPs and shows that a hydrophobic environment is a key factor in promoting the $[Fe_4S_4(Cys)_4]^{1-}$ level because there are few or no polar groups available to dissipate higher net charges on the cluster.

In *Cv* HiPIP, the single Fe_4S_4 cluster is buried in the center of the protein, and the cluster is at a considerably greater distance from the protein surface than in the Fds.[5,7b] In our Raman studies, deuterium exchange of the amide NH groups hydrogen bonded to cysteine ligands was observed only after partial unfolding of the protein. Native *Cv* HiPIP showed no exchange after 7 days of incubation in D_2O, whereas native *Cp* and *Ca* Fds showed complete exchange after only 1 day of incubation in D_2O. Protons that fail to exchange with solvent in days to weeks are typically located in buried, nonpolar interior regions of proteins.[42] Thus, our results prove that the cluster environment in HiPIP is considerably more hydrophobic than in Fd and does not undergo enough breathing motion to allow water molecules access to the cluster. As in the case of the model complexes, this type of nonpolar environment selects for the less charged cluster oxidation state of 1− in HiPIPs.

The smaller number of cluster hydrogen bonds in HiPIP than in Fd presumably helps to favor a higher oxidation level in HiPIP. However, hydrogen bonding of sulfur ligands in proteins is also important to the achievement of particular active-site conformations.[19] In the mononuclear $Fe(Cys)_4$ rubredoxins from *Desulfovibrio vulgaris*, *D. gigas*, and *C. pasteurianum* there is a strong conservation of the polypeptide structure surrounding the iron–sulfur center, including six totally conserved hydrogen bonds to the cysteine ligands.[39b,c] The eight conserved hydrogen bonds in the Fe_4S_4 ferredoxins must also be essential for structure stabilization. The role of the iron–sulfur clusters in promoting protein folding can be seen from the markedly increased susceptibility of apoferredoxin to proteolytic digestion[52] and from the evolution of an additional α-helical element to compensate for the loss of cluster II in *Dg* and *Bt* Fds.[11a] Similarly, the five hydrogen bonds to the $Fe_4S_4(Cys)_4$ cluster in *Cv* HiPIP are likely to be providing necessary structural support. They may represent a compromise between maximal hydrogen bonding for structural stability and minimal hydrogen bonding to achieve a higher cluster oxidation level.

The ~400-mV range in redox potential among HiPIPs must again be due to microenvironmental effects, as in the case of Fds and cytochromes *c*. Amino acid sequence homologies and ^1H NMR spectra indicate that HiPIPs have conserved protein structures,[53] suggesting that the iron–sulfur cluster will be similarly inaccessible to solvent in all cases. Resonance Raman spectra of HiPIPs show that the cluster geometry and coordination to the protein is also highly conserved. The wide variations in *surface* charge (e.g., 3+ for *Rt* and 4− for *Cv* HiPIP) have a negligible contribution to redox potential (330 and 360 mV, respectively),[5] as can also be seen from the fact that the E_0' of *Cv* HiPIP is essentially unaffected by changes in ionic strength.[54] Thus, differences in the polarity and electron-delocalizing ability[55] of amino acids in the vicinity of the cluster are likely to be major

(44) (a) Churg, A. K.; Warshel, A. *Biochemistry* **1986**, *25*, 1675–1681. (b) Moore, G. R.; Pettigrew, G. W.; Rogers, N. K. *Proc. Natl. Acad. Sci. U.S.A.* **1986**, *83*, 4998–4999. (c) Kassner, R. J. *J. Am. Chem. Soc.* **1973**, *95*, 2674–2677.

(45) Cutler, R. L.; Davies, A. M.; Creighton, S.; Warshel, A.; Moore, G. R.; Smith, M.; Mauk, A. G. *Biochemistry* **1989**, *28*, 3188–3197.

(46) Varadarajan, R.; Zewert, T. E.; Gray, H. B.; Boxer, S. G. *Science* **1989**, *243*, 69–72.

(47) Ciurli, S.; Carrié, M.; Weigel, J. A.; Carney, M. J.; Stack, T. D. P.; Papaefthymiou, G. C.; Holm, R. H. *J. Am. Chem. Soc.* **1990**, *112*, 2654–2664.

(48) Navarro, J. A.; Cheddar, G.; Tollin, G. *Biochemistry* **1989**, *28*, 6057–6065.

(49) (a) Hill, C. L.; Renaud, J.; Holm, R. H.; Mortenson, L. E. *J. Am. Chem. Soc.* **1977**, *99*, 2549–2557. (b) Tanaka, K.; Tanaka, T.; Kawafune, I. *Inorg. Chem.* **1984**, *23*, 518–519.

(50) O'Sullivan, T.; Millar, M. *J. Am. Chem. Soc.* **1985**, *107*, 4096–4097.

(51) (a) Nakamoto, M.; Tanaka, K.; Tanaka, T. *J. Chem. Soc., Chem. Commun.* **1988**, 1422–1423. (b) Okuno, Y.; Uoto, K.; Yonemitsu, O.; Tomohiro, T. *J. Chem. Soc., Chem. Commun.* **1987**, 1018–1020.

(52) Skjeldal, L.; Draget, K.; Ljones, T. *Biochim. Biophys. Acta* **1989**, *995*, 59–63.

(53) Krishnamoorthi, R.; Cusanovich, M. A.; Meyer, T. E.; Przysiecki, C. T. *Eur. J. Biochem.* **1989**, *181*, 81–85.

(54) Mizrahi, I. A. Ph.D. Dissertation, University of Arizona, 1977.

(55) Sola, M.; Cowan, J. A.; Gray, H. B. *Biochemistry* **1989**, *28*, 5261–5268.

factors influencing the redox potential in different HiPIPs.

Conclusions

(1) The X-ray structures of *Pa*, *Av*, and *Bt* ferredoxins show that the geometry of the $Fe_4S_4(Cys)_4$ cluster and the surrounding polypeptide chains are highly conserved. Thus, the ~400-mV range in redox potentials *cannot* be ascribed to differences in the Fe_4S_4 structures, cysteine torsional angles, or amide hydrogen bonding to sulfur atoms. Rather, the redox potentials are likely to be reflecting different amino acid side chains in the vicinity of the cluster and different degrees of exposure of the clusters to solvent. These results suggest that redox potentials are influenced by the dynamic as well as the static structures of proteins. Further proof of this hypothesis must await careful site-directed mutagenesis studies coupled with high-resolution structure determination and electrostatic field calculations.

(2) Resonance Raman spectra of HiPIPs from *Cv*, *Rt*, *Rg*, and *Eh* in both their oxidized and reduced states reveal that the structures of their $Fe_4S_4(Cys)_4$ clusters are also highly conserved and likely to be similar to one another in Fe_4S_4 geometry and cysteine torsional angles. Although differences in hydrogen bonding cannot be ruled out, it is likely that the ~350-mV range in redox potentials is due primarily to microelectrostatic environmental effects, as in the ferredoxins.

(3) A comparison of ferredoxins and HiPIPs by X-ray crystallography and RR spectroscopy reveals that the iron–sulfur clusters in both cases have similar D_{2d}-distorted Fe_4S_4 geometries. They do differ in the number of amide hydrogen bonds to sulfur ligands (eight in Fds, five in HiPIPs) and in the degree of solvent accessibility of the cluster (hydrogens more exchangeable in Fds than in HiPIPs). Both of these factors may contribute to the destabilization of the 3- oxidation level in HiPIPs, making the 1-/2- couple more feasible than in ferredoxins.

(4) Raman spectroscopy is proving to be a sensitive indicator of the $Fe-S_\gamma-C_\beta-C_\alpha$ dihedral angles of cysteine ligands. When dihedral angles are close to 180°, as in HiPIPs, but not in Fds, there is an increased number of Fe–S(Cys) vibrational modes as well as an increase in their vibrational frequencies. Such differences in ligand dihedral angles are also capable of influencing the redox potentials of metal centers.[56]

Acknowledgment. We thank Drs. A. Grant Mauk, Nanette R. Orme-Johnson, Jean-Marc Moulis, and Michael T. Ashby for helpful comments, Dr. Charles W. Carter, Jr., for providing coordinates of the refined HiPIP structures, and Martin Gluck for preparation of the ferredoxin samples. This research was supported by the U.S. Public Health Service, National Institute of Health Grants GM 18865 (T.M.L. and J.S.-L.) GM 21277 (M.A.C.), GM 27382 (W.V.S.), and GM 31770 (E.T.A.).

(56) Chang, C. S. J.; Collison, D.; Mabbs, F. E.; Enemark, J. H. *Inorg. Chem.* **1990**, *29*, 2261–2267.